MSUCP-26

MICHIGAN STATE UNIVERSITY

CYCLOTRON PROJECT

Phase Selection Mechanisms in Isochronous Cyclotrons Producing High Resolution Beams*

J.C. Collins

Department of Physics - Cyclotron Laboratory

East Lansing, Michigan

August, 1973

*This work was partially supported by the National Science Foundation

ACKNOWLEDGEMENTS

I would like to take this opportunity to thank Julie Perkins for invaluable help and advice in the preparation of this manuscript.

I would also like to thank Richard Au and Dave Johnson for their time and aid in computer programming and the use of orbit codes.

Thanks are due also to Larry Learn and Dr. Henry Blosser for many helpful discussions and explanations of cyclotron theory and operations.

My special thanks go to Dr. Morton Gordon whose patient guidance gave this work direction and purpose and to my wife Carolyn, whose impatient prodding kept the work moving along. This thesis could not have been finished without both of these people.

Finally, I wish to acknowledge the financial support of the National Science Foundation throughout my graduate career.

LIST OF FIGURES

variation of the accelerating voltage with time but, while possibly larger than desired, this would be much smaller than the energy gain per turn. The fractional energy spread generated in this way for a beam phase width of $2\Delta\phi$ in a perfectly isochronous field is:[1]

$$\Delta E/E = (\Delta\phi)^2/2. \qquad (1)$$

From extensive studies,[2] it was confirmed that single turn extraction requires small $\Delta\phi$. Not independently one notices from Eq. (1) that this also produces superior energy resolution. The question then is how to obtain such small phase widths.

Three methods have been used to accomplish this selection of desired phase at M.S.U. The original idea was to use the phase dependent axial focusing properties of the electric field at the first few gaps with an axial slit.[3] This system produced phase widths of about 7^o, good enough to observe single turn extraction. However, Eq. (1) indicates that it is profitable to attempt to reduce this phase width as much as possible. It was also true that the axial slit passed particles of any phase if they were emitted with small axial momentum near the median plane. Analysis of certain empirical data showed that radial slits at the half and tenth turns gave better phase selection.[4] Such a system worked through the coupling between the radial and longitudinal (E-ϕ) motions of the

1.2 The Approach to the Problem

The data presented herein is intended as only a very rough guide to the importance of the parameters investigated and the effectiveness of phase selection slits under specified conditions. We have neglected details of source and early turn electric fields which would have important consequences in real cyclotrons but which would also be different in every machine. What we wish to emphasize are the methods we use to analyze the longitudinal-radial coupling since these apply universally and serve as a very handy visualization of the coupling process.

The inclusion of phase selection slits allows us to define a central ray from ion source to extractor. This is done in Sec. 2.1. This central ray plays a crucial role in this analysis, as it does in the design and operation of any cyclotron built for high resolution. From one point of view, a real beam is built up around the central ray through small variations in position, momentum and phase, so that beam properties in general and the properties of individual particles in the beam should be intimately related to the characteristics of the central ray.

We investigated various dee angles between 180° and 90° since most existing cyclotrons use 180° dees with some (Maryland being the prime example) using 90° dees and a few using 150° or 120° dees. Both three and four sector magnetic fields are used and acceleration harmonics one, two and three were looked at. Other parameters

2. ORBIT PROPERTIES AND CALCULATIONS

2.1 Introductory Mechanics

To facilitate the study of particle orbits and their differences, we may resolve the radial position of a particle of energy E at azimuth θ, $r(E,\theta)$, into two components. The first is the static equilibrium orbit (EO) radius, $R_{EO}(E,\theta)$; the second is the deviation from that EO value

$$x = r(E,\theta) - R_{EO}(E,\theta).$$

For any energy E we may define the EO in a magnetic field as the non-accelerated closed orbit having the same periodicity as the field. This analysis proves useful because the EO is a function only of azimuth and total energy (see Sec. 2.5). Thus we may separate out purely energy effects in the radial differences between particles. The canonically conjugate variable, p_r, the radial component of momentum, is likewise resolved such that

$$p_x = p_r(E,\theta) - P_{REO}(E,\theta).$$

Of course, x and p_x are also functions of energy and azimuth, but we choose not to include that dependence in our notation. Since x and p_x have equal footing in this formulation, it is highly convenient to express them in the same units.

fields, partly because one may visualize x and p_x values as specifying the deviation of the actual particle orbit center from the magnetic field center, and partly because one can show that a particle coasting in the vicinity of a reference EO of the same energy executes harmonic (betatron) oscillations about that EO.[6] In the x-p_x plane centered on this EO, the phase point for the coasting particle rotates about the origin at a distance equal to the precessional oscillation amplitude and at a rate such that, at a given azimuth the phase point returns to its original position after $1/(\nu_r-1)$ orbits (turns) in the field. If one observes the location of such a phase point over many turns at a fixed azimuth relative to each field sector, one finds that an eigen-ellipse is traced out. The ellipse is a function of azimuth arising from the periodicity of the magnetic field through Floquet's theorem. Detailed accounts of its properties may be found elsewhere,[7,8,9] and will not be reproduced here. As an example, one such ellipse is traced out in Fig. 1a for a proton of 14 MeV coasting in a field corresponding to a maximum energy of 30 MeV. (See Sec. 2.2 for the source of this field.) Initial conditions used are x=20 mils and p_x=0 mils and $\nu_r \simeq 1.05$.

Since particles execute betatron oscillations about any orbit which satisfies the equations of motion in the given field, we are not limited to the static EO as our

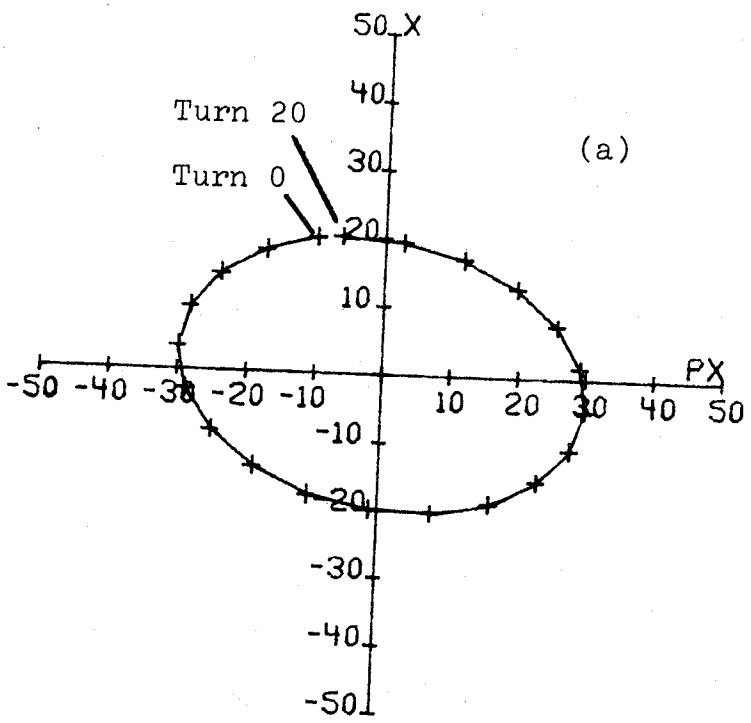
50 X
40
30
20
10
-10
-20
-30
-40
-50
Turn 20
Turn 0
(a)
PX
-50 -40 -30 -20 -10
10 20 30 40 50

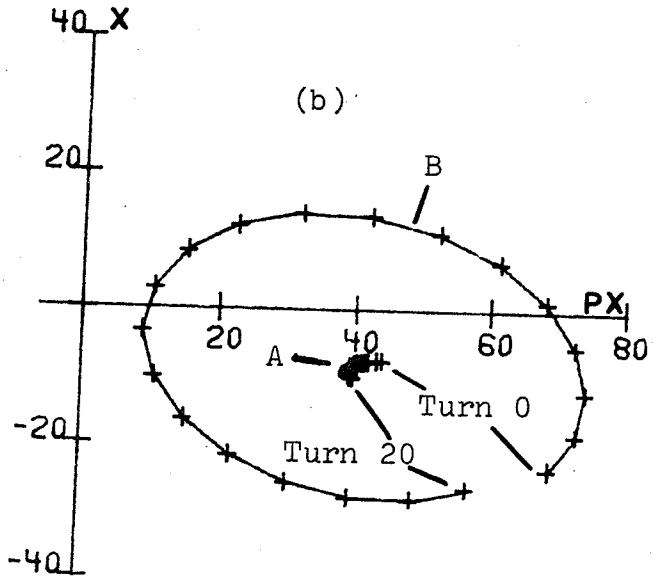
40 X
20
-20
-40
(b)
B
A
Turn 0
Turn 20
PX
20 40 60 80

Figure 1.

radial oscillations as B traverses the path shown for it. The beam ellipse centered on A would effectively occupy an area only slightly larger than itself since A does not move far in the $x\text{-}p_x$ plane. This is true regardless of incoherent variations inside each ellipse. The beam corresponding to the ellipse centered on A may be termed "well-centered". In fact, at a given energy and phase, the beam centered on the appropriate AEO will show the minimum possible coherent oscillation amplitude. While this condition holds exactly at only one energy, the coherent oscillation amplitude increases only slowly with deviations from the energy of the selected AEO, so that a beam which is well-centered near the middle of its acceleration history will be so throughout its entire history except on the first few turns after the source-puller. Such centering is of great practical importance because it reduces phase oscillations (see Sec. 2.4), minimizes the effects of non-linearities and makes extraction insensitive to dee voltage.

Like the EO, the AEO depends on the magnetic field. But since the AEO characterizes the acceleration process, it is also a function of the dee structure and the particle phase, of which properties the EO is independent. Details of AEO properties of specific importance to this study are given in Sec. 2.3.

2.2 Computation Technique

The information provided above may now be used to guide our design of the calculations required to understand the longitudinal-radial coupling. We are certainly interested in EO and AEO properties as well as in finding a well centered beam. We are also interested in determining how machine design affects these properties and, through them, phase selection. The discussion below of the codes and calculation methods finally used serves to list and fix some limitations on the machine parameters at our disposal, as well as showing how the concepts of the AEO and well centered beam are actually put to use.

Most of the magnetic fields used were obtained using the field trimming program "Fielder".[10] Two Fielder features are particularly convenient for studying the various effects of phase histories: (a) one may specify a desired phase-as-a-function-of-energy curve to which the final field should conform; and (b) an acceleration history of phase and energy vs. turn number (τ) is output along with the field. The phase history, denoted $\phi_F(\tau)$ or $\phi_F(E)$, is quite valuable for estimating one contribution to the longitudinal-radial coupling as shown in Sec. 2.5. It is obtained by assuming that the particle gains energy continuously and always remains on an EO. This is a good approximation for a well centered particle when its energy is very much greater than the maximum energy gain per turn.

M.S.U. field data, $\theta=0^{o}$ is positioned near the center of a valley. For convenience we number the accelerating gaps counterclockwise beginning with gap 1 at

$$\theta_1 = \theta_{or} + (\pi-\alpha)/2$$

$$\theta_2 = \theta_{or} + (\pi+\alpha)/2$$

$$\theta_3 = \theta_1 + \pi$$

$$\theta_4 = \theta_2 + \pi.$$

The codes used to calculate particle orbits all use the same exact median plane equations of motion and assume step function energy gain. This assumption is a limitation in applying our quantitative results directly to any real machine if the first few acceleration gaps are included. There, transit time effects are important as they modify the CR x-p_x and phase (energy gain) histories. These effects are so highly dependent on central region geometry, it was thought best to omit them entirely from this work.

The particles are assumed to start from a virtual source at $\theta=\theta_1$ on the first turn ($\tau=0$). We consider 0.9 times the maximum energy gain per gap, E_g, to be a reasonable source-puller or axial injection energy and use this value in step iii) below.

The outline of our calculational procedure is as follows:

i) We obtained a magnetic field from Fielder. The input to Fielder consisted of the field periodicity N,

iv) With the initial CR coordinates (r_i, p_{ri}, ϕ_i, E_i) now determined, we used the code "Devil", written by the author (see Sec. 5.2), to accelerate the CR and rays differing from it slightly by δr_i, δp_{ri} and/or $\delta \phi_i$. Devil output the orbit properties (r, p_r, ϕ, E, x, p_x) at each dee gap and any other azimuths desired (usually θ_{or} and $\theta_{or}+\pi$) along with the differences in r, R_{EO}, x and p_x between the CR and the displaced rays. This output forms the great majority of the data displayed in this thesis.

to our understanding of the AEO, so we shall not treat it specifically. The transfer matrix used here neglects all field structure and is symmetric between half turns, that is, after one half turn, $x=x_o$ and $p_x=p_{xo}$.

Figures 2 and 3 show Disport-2 results for AEO's in 30 MeV proton fields with N=4 and N=3, respectively. The AEO properties are plotted vs. energy at $\alpha=138^o$ and vs. dee angle at E=7.5 MeV, both at $\theta=\theta_{or}=0^o$. We plot the average in mils of the p_x values at $\theta=0^o$ and 180^o for comparison with Eq. (2). The average x values are not included as they never exceed 1.5 mils. To measure orbit asymmetry, i.e., the deviation from Eq. (2), we plot the deviations from the average in x and p_x values at $\theta=0^o$. The x deviations have sign opposite that of the other quantities plotted.

The results in the four sector field are in excellent agreement with Eq. (2) using δ varying as $(\Delta E)\ E^{-\frac{1}{2}}$, where ΔE is taken as the energy gain per turn divided by the number of acceleration gaps (see Sec. 2.5). The asymmetries are quite small, except at rather low energies where the assumption of constant δ begins to fail markedly. Such agreement with Eq. (2) is not too surprising since the field and dee geometries are both symmetric between half turns.

AEO's in a three sector field (Fig. 3) are quite asymmetric, however. Numerical agreement with Eq. (2) is quite poor for both dee angle and energy dependence. Obviously, Eq. (2) makes no allowance for the fact that the

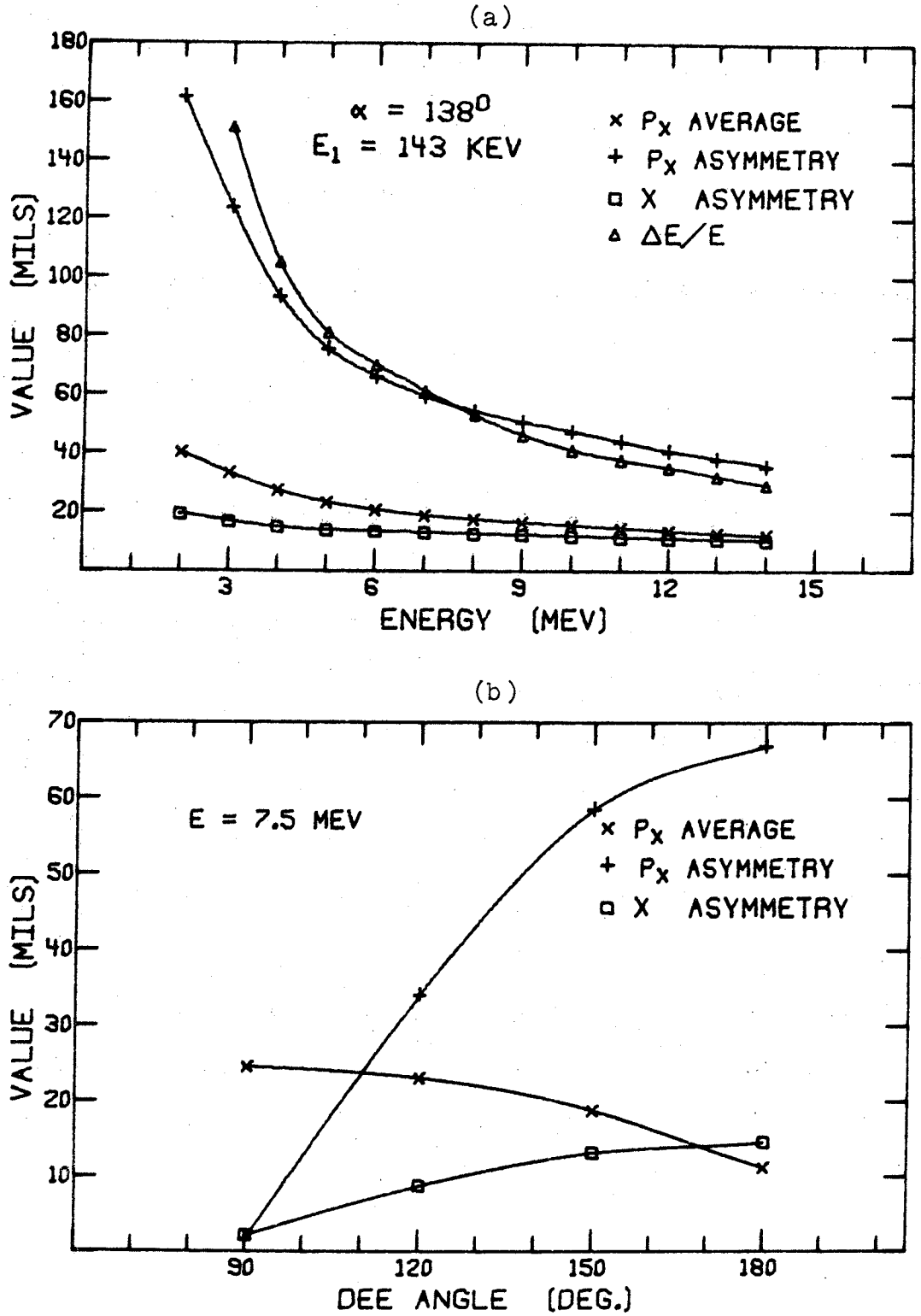

Figure 3. AEO properties as in Fig. 2 except with a three sector magnetic field. Compare the ordinate scales with those in Fig. 2.

Figure 4.--X-P_x history of the first 50 turns for a well centered proton with $\alpha=138^{o}$, $E_f=30$ MeV, $E_1=143$ keV/turn, N=3, h=1. Every turn is given (dot) to $\tau=5$ (circled) with every fifth turn shown thereafter. Crosses mark AEO locations at 10 turn intervals beginning at $\tau=5$. All axes are in mils.

δp_x=23 mils for τ=7, δx=17 mils, δp_x=-8 mils for τ=28 and δx=10 mils, δp_x=3 mils for τ=49. Starting from this history, one can easily justify the locations of the other histories by assuming that a phase point rotates counter-clockwise about the origin by an angle nearly equal to that through which the actual particle coasts between gaps and including the acceleration dependent shifts in the negative x direction at each gap.

Increasing θ_{or} from 0^o to 30^o gives Fig. 4b which may be related to Fig. 4a by reversing the roles of x and p_x. This is a direct consequence of the exchange of x and p_x asymmetry values for AEO's under the same dee rotation. These asymmetry values also account for the inequality between p_x (x) values at gaps 1 and 4 and those at gaps 2 and 3 in Fig. 4a and c (b and d). Further increments of 30^o in θ_{or} give Fig.'s 4c and d which are quite similar to Fig.'s 4a and b with a reversal in gap labels.

The second CR characteristic of interest is its phase history at each gap and the relation between these histories and $\phi_F(\tau)$. A sample set of phase histories may be found in Fig. 5a-d for the same four cases as Fig. 4a-d while the corresponding $\phi_F(\tau)$ is labeled 'C' in Fig. 17 page . There are two effects which cause deviations between $\phi_F(\tau)$ and actual CR phase histories, ϕ_{CR}. Of lesser importance is the form factor effect. In a sectored field the EO's are scalloped, a consequence of which is that the EO path

length is greater in the hills than in the valleys. Particle phase tends to increase while crossing hills and decrease while crossing valleys. For h=1, the phase oscillation amplitude thus produced is of the order of only one degree. This amplitude is directly proportional to h and becomes more important with higher harmonic operation.

Of greater importance are those deviations arising because the actual orbit center does not correspond to the field center, i.e., because x and p_x differ from zero. In general, one can show that the centering dependent phase shift involved with traversing an angle β may be well approximated by

$$\delta\phi_{CD} \simeq h(p_x(1-\cos\beta) + x(\sin\beta))/R_o \qquad (3)$$

where R_o should be taken as an average orbit radius and x and p_x pertain to the beginning of the angle in question. Note that $\delta\phi_{CD}$ is expected to be large only at small radii and that p_x carries the greater weighting factor if $\beta>\pi/2$ and so will usually be of greater importance than x in determining $\delta\phi_{CD}$. Since $\delta\phi_{CD}$ may easily be many degrees on early turns even for h=1, we see that there is an intimate and important connection between the centering of a particle and its phase history.

In particular, we may inspect an x-p_x history, such as Fig. 4a, and predict the $\delta\phi_{CD}$ occurring between any two dee gaps with Eq. (3). Table I contains such predictions

The remaining three phase curve sets of Fig. 5 may likewise be explained using the corresponding $x\text{-}p_x$ history of Fig. 4. We take this opportunity to point out that, since the histories of Fig. 4 are qualitatively representative of all three sector field cases to be discussed below, the phase histories of Fig. 5 may likewise be considered to have all the qualitative features found in any case of interest in a three sector field.

Similar data for a four sector field is found in Fig.'s 6 and 7 respectively. Note how rapidly the crosses representing AEO's approach the origin in Fig. 6a so that only for τ=5 and 15 are they clearly visible. The cross locations are the same in Figs. 6b-d as in Fig. 6a and so are not included. The highly symmetrical AEO's give rise to very well centered beams at all dee angles, so the $\delta\phi_{CD}$'s are quite small. This implies that, in contrast to the three sector case, the relative field-dee orientation will have practically no effect on the phase histories, as inspection of Fig. 7 immediately verifies.

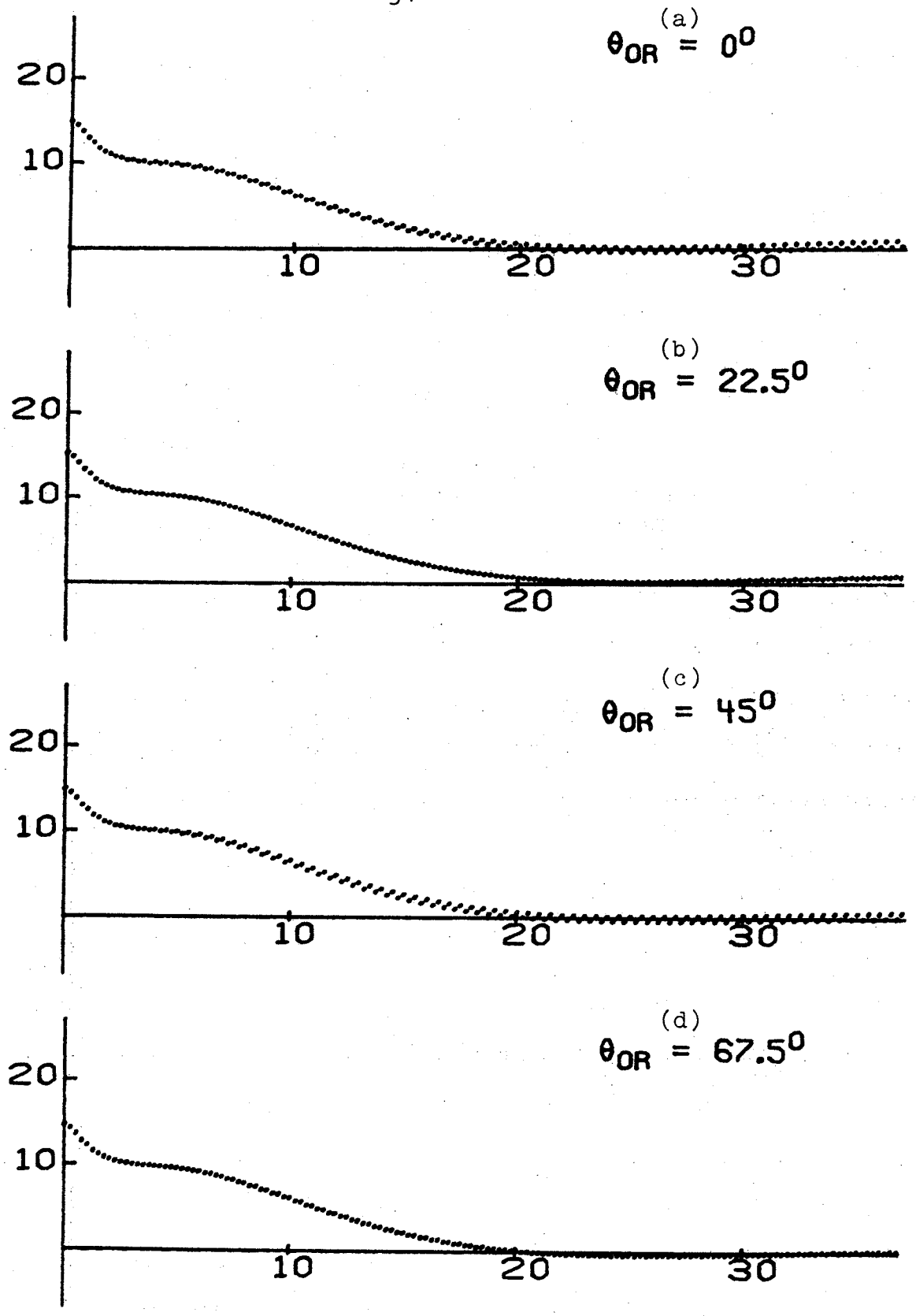

Figure 7. Phase history (deg vs. τ at each gap) for the cases shown in Fig. 6. Note that gap crossing phase is unaffected by θ_{or}, unlike in Fig. 5.

Let us start with ΔR_{EO}. It is a straight-forward job to determine that

$$R_{EO}(E,\theta) = R_o(E)(1 + F(\theta)) \tag{5}$$

describes the EO of energy E in a periodic magnetic field where

$$R_o(E) = A(2E/E_o)^{\frac{1}{2}}, \tag{6}$$

$F(\theta)$ being the orbit form factor having the same periodicity as the field.[13] This description assumes that the field is isochronous and that the energies are not relativistic. Actually, $F(\theta)$ is also a function of energy, but as long as this dependence is weak (the case in all our fields) we will suppress it, giving us a simple formula for the change in the EO with an energy change δE:

$$\Delta R_{EO}(E,\delta E,\theta) \simeq A(\delta E)(2EE_o)^{-\frac{1}{2}}(1 + F(\theta)). \tag{7}$$

A good first order approximation for the energy difference between phase displaced rays after any number of complete turns is

$$\Delta E = -E_1(\Delta\phi)\int_0^{\tau}\phi_F(\tau')d\tau' \tag{8}$$

(see Sec. 5.1.2) where $\Delta\phi$ is the initial ray phase separation. The accuracy of Eq. (8), will be tested numerically in Chapter 3. Its usefulness arises because, in conjunction with Eq. (7), it may be used as a very simple method of estimating the EO component of ΔR in Eq. (4).

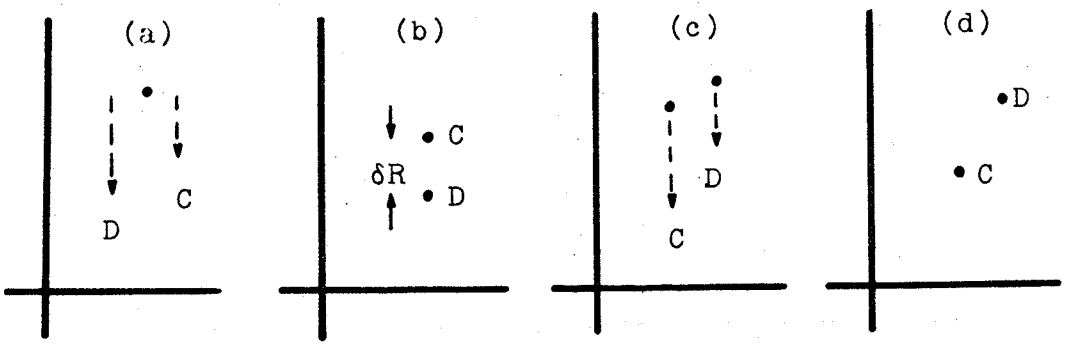

Figure 8. Schematic representation of the growth of Λ between the CR (point C) and a phase displaced ray (point D). (See text, p. 37.)

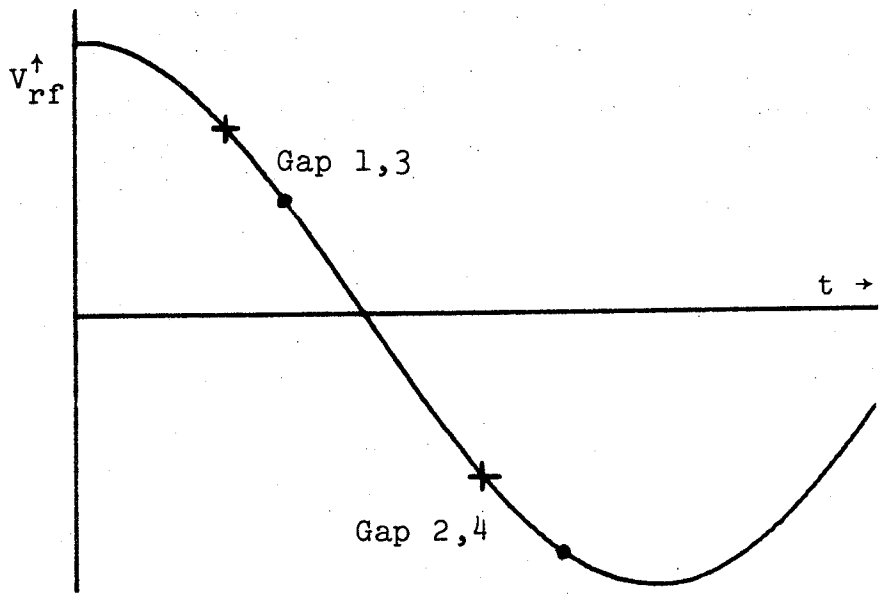

Figure 9. Difference in rf times of gap crossings for zero (crosses) and non-zero (dots) phases for h=1.

between the dot and cross for a given gap translates directly into a difference in disjunctive effects between gap pairs. We shall term this the rf asymmetry effect.

Furthermore, in any four gap situation, the net change in Λ over one turn as measured at $\theta=\theta_{or}$, for example, is

$$\Delta\Lambda = (\Delta\lambda_{13})K_1 + (\Delta\lambda_{24})K_2. \qquad (9)$$

The K_1 and K_2 are vectors depending on the dee angle since, to first order, they would parallel the respective gap pairs. But K_1 and K_2 are not simple to calculate accurately since they also depend on the past acceleration history of Λ. The disjunction at an intervening gap effectively changes the angle of rotation of Λ from the expected value of nearly 180^{o} between opposing gaps, a change which must be reflected in K_1 and K_2. We shall refer to Eq. (9), linking the net disjunctions at each pair of opposing gaps to the change in Λ per turn, as defining the gap-pair coupling effect.

We now can see that it would be quite difficult to calculate this second component of ΔR. To obtain an expression like Eq. (5) for λ or Eq. (7) for $\Delta\lambda$, one would need an analytical form for the phase as a function of gap and turn numbers, which is not readily available ($\phi_F(\tau)$ is absolutely inadequate for this), and a similar form for the vectors K_1 and K_2 in Eq. (9) above.

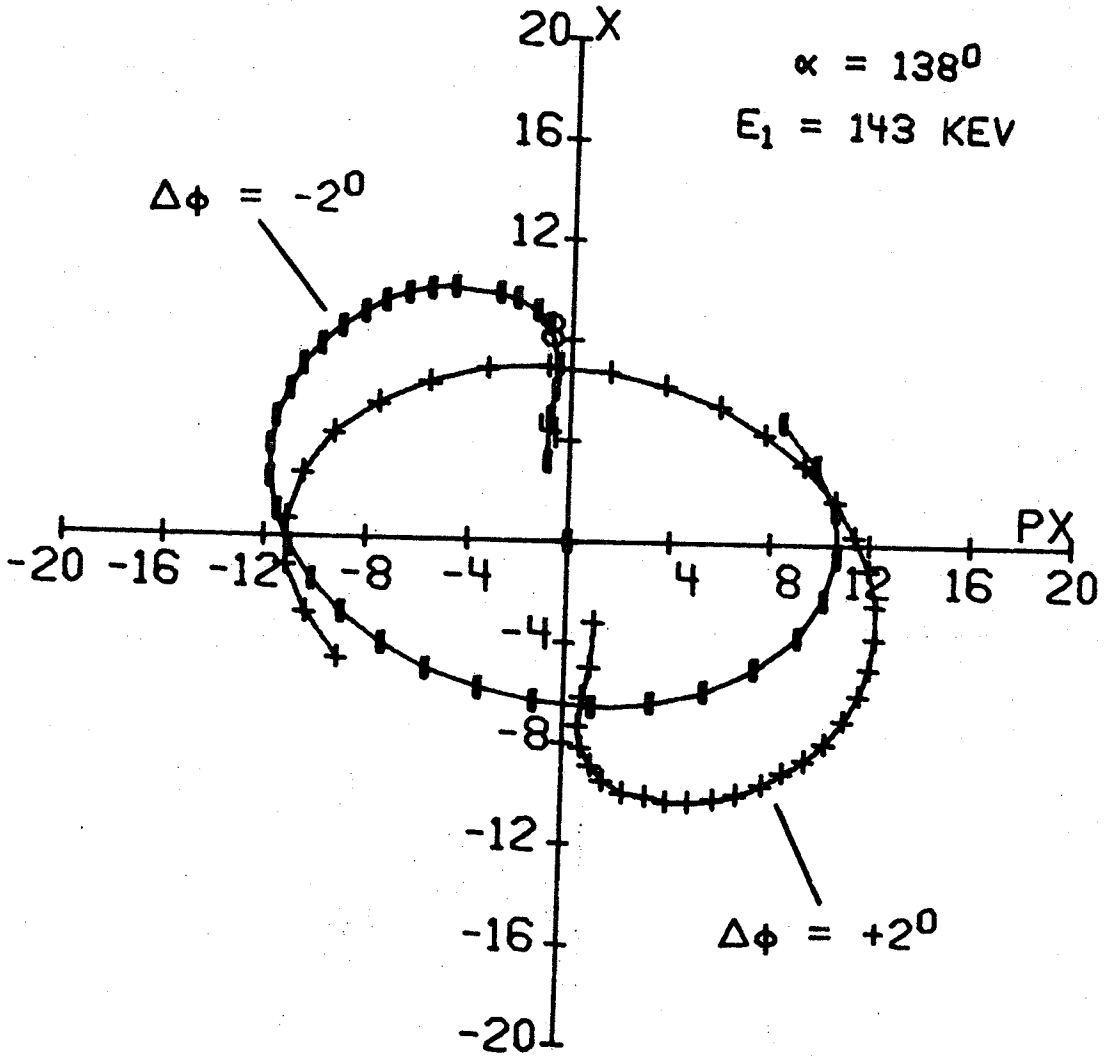

Figure 10. δx-δp_x history for the first 40 turns for rays with $\Delta\phi=\pm 2^{\circ}$. Properties of the reference CR are shown in Figs. 4a and 5a. Points are plotted once per turn at $\theta=\theta_{or}=0^{\circ}$. All axes are in mils.

We shall regard Q as constant with respect to $\Delta\phi$ in any given situation. Orbit calculations show that, for most cases below, this is true for $\Delta\phi$ as large as 32^{o}. Even for the exceptional cases, Q may easily be assumed to be constant over the small $\Delta\phi$ we would expect a practical slit to pass.

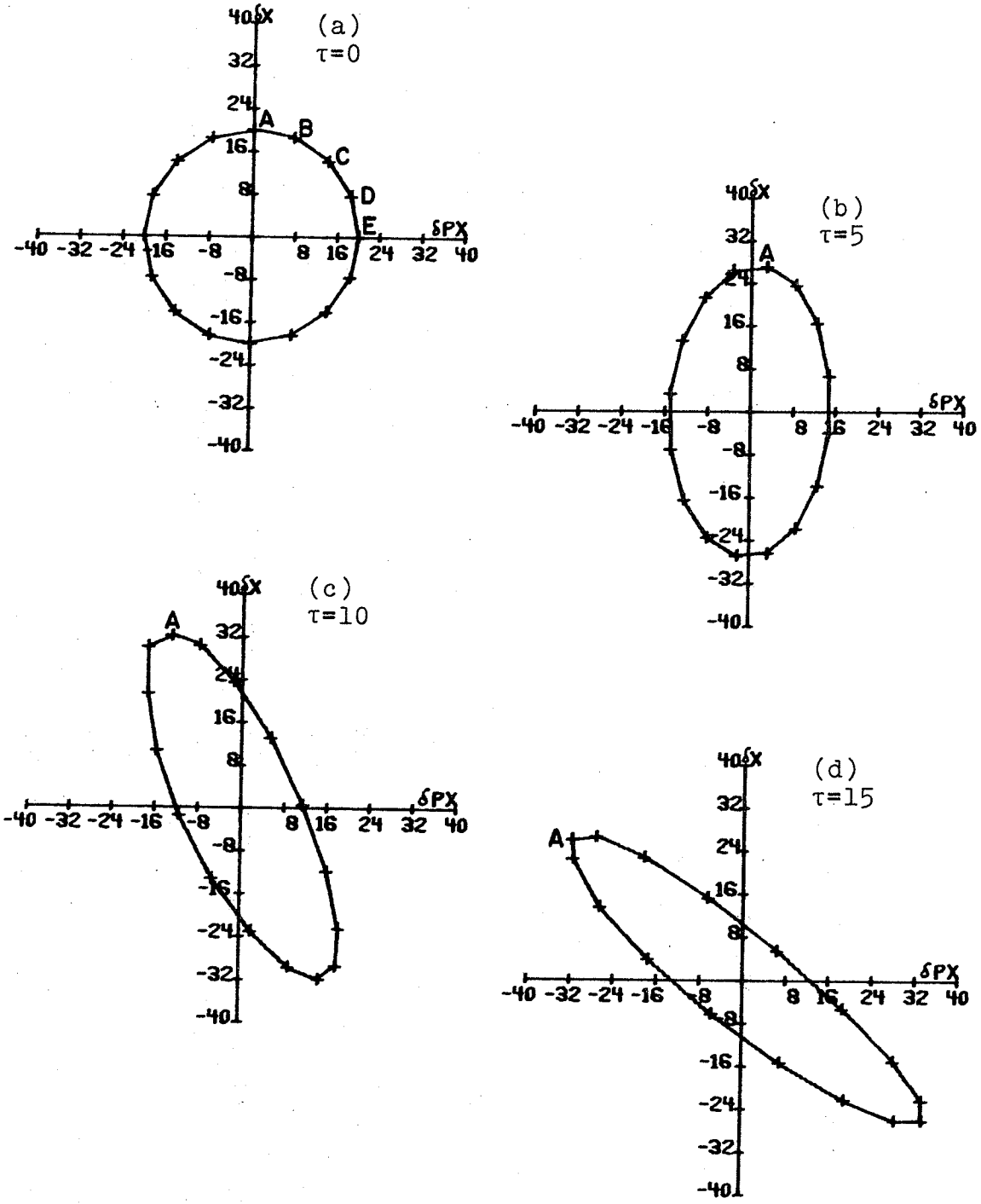

Figure 11. δx-δp_x history for 16 rays initially located on a circle of 20 mil radius. Properties of the reference CR are shown in Figs. 4a and 5a. All axes are in mils.

(Fig. 1f). The distortion of the original (arbitrary) circular shape may be seen to be essentially complete by τ=15 and the resultant beam ellipse mainly rotates thereafter. A nice explanation of this phenomenon has been given by Bolduc and Mackenzie.[14] The occupied area on the δx-δp_x plane varies from 1256 mils^2 at τ=0 to nearly 1200 mils^2 at τ=15, a pleasing result since the accompanying δE-$\delta\phi$ co-ordinate changes are small.

There is a fixed relationship between the orientation of the ellipses in Fig. 11 and the phase oscillations of Fig. 12 such that, for a given ray, the turn where its extreme δp_x value occurs corresponds to the turn with an extremum in its $\delta\phi$. Finally, note that, just as the rays of larger δx_o experience larger distortions in the δx-δp_x plane, so do they also show larger oscillations about their $\delta\phi_{av}$ ($\sim$0.3^o with $\sim$0.3^o average shift).

While we will emphasize the effects of temporal over spatial displacements in this paper, we will present some data pertinent to the behavior of rays with the initial conditions used above for Fig. 11. We should, therefore, establish whether the effects we see are linear with δx_o and δp_{xo}. Figure 13 gives values of $(\delta x^2 + \delta p_x^2)^{\frac{1}{2}}$ between the CR and the ray marked 'A' in Fig. 11 as functions of initial δx_o and δp_{xo} for three different dee angles. For values of 150 to 200 mils one observes deviations from linearity, especially for 90^o dees, but for smaller values

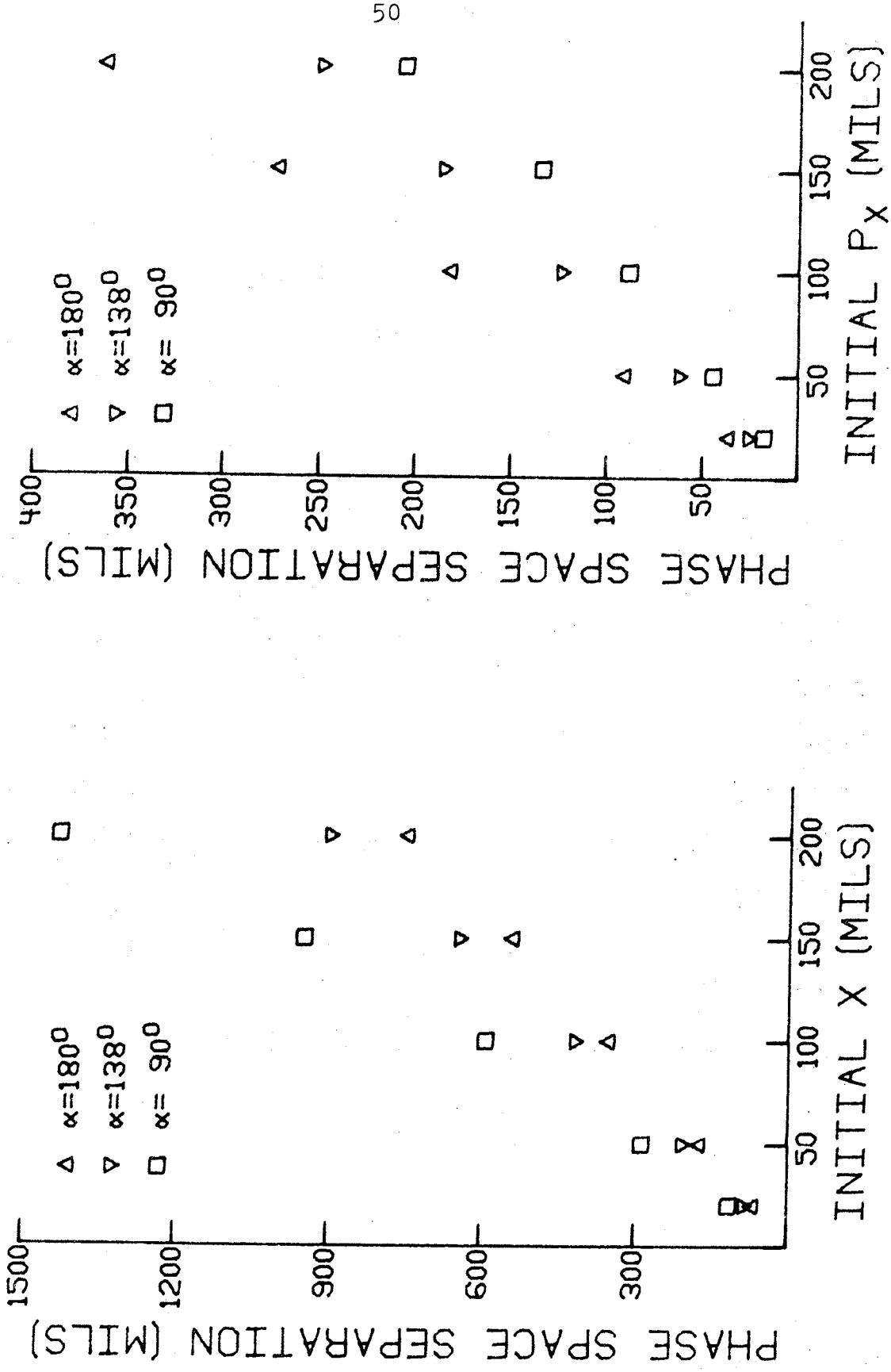
PHASE SPACE SEPARATION (MILS)
INITIAL X (MILS)
INITIAL P_X (MILS)
α=180°
α=138°
α= 90°
1500
1200
900
600
300
400
350
300
250
200
150
100
50
50
100
150
200

Figure 13.

under discussion show very small ΔR_{EO} values. In fact, the rate of increase of ΔR_{EO} with δx_o and δp_{xo} is about an order of magnitude less than that shown in Fig. 13 for the increase in phase space displacement.

We make these comments by way of explaining that the radial separation between the CR and spatially displaced rays is insensitive to the parameters in Chapter 3 except for h, the effect of which is summarized in Table II. Therefore, we present no further data on such rays in Chapter 3. We will, however, return to this subject when the question of locating phase selective slits arises in Chapter 4.

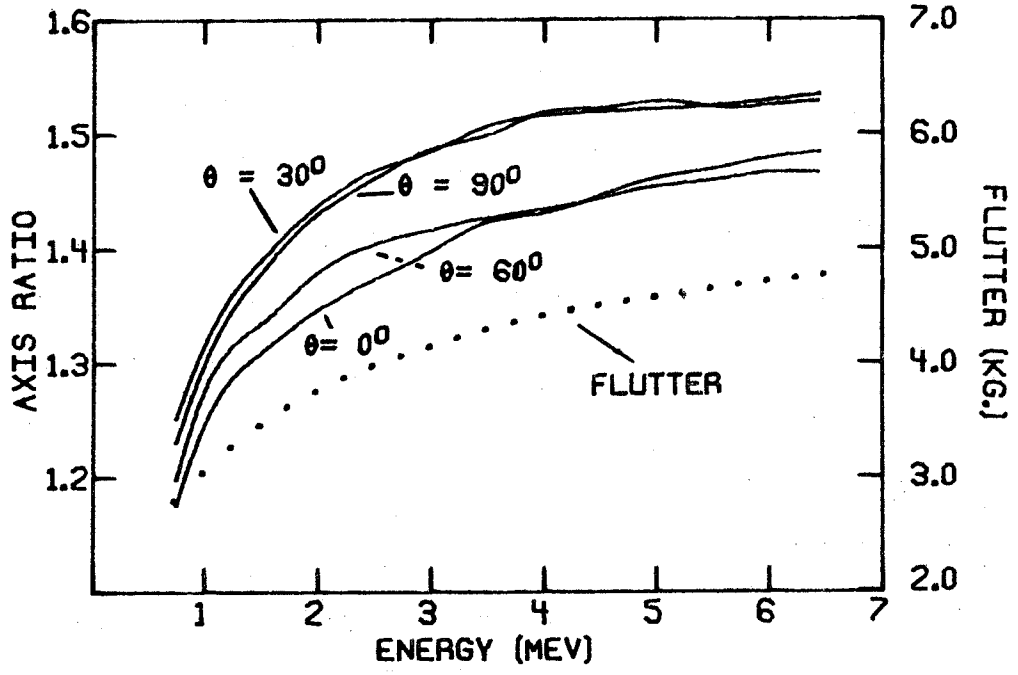

Figure 14. Eigen-ellipse axis length ratios and flutter vs. energy for an M.S.U. proton field with N=3, E_f=30 MeV.

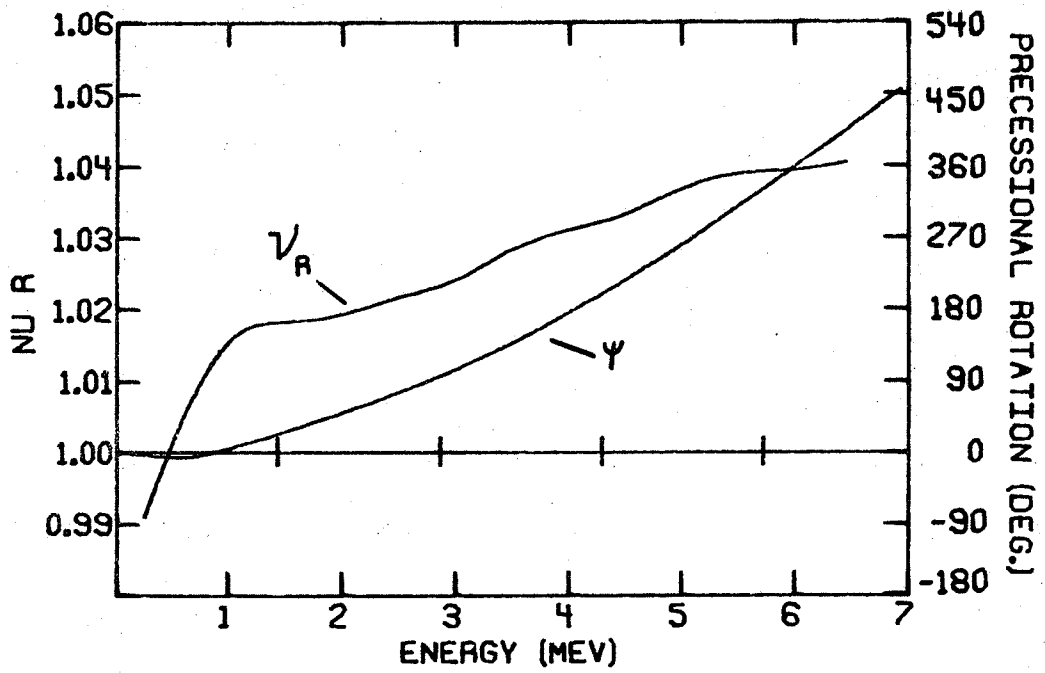

Figure 15. ν_r and ψ(see Eq. 11) vs. energy for the field of Fig. 14.

TABLE III.--ΔE and ΔR_{EO} at $\theta=\theta_{or}$ and $\theta=\theta_{or}+\pi$ for various dee angles. The magnetic field used corresponds to curve C in Fig. 17.

N=3 h=1 E_1=143 keV/turn $\Delta\phi=\pm2^\circ$

τ	θ_{or}	α=180 ΔE (keV)	α=180 ΔR_{EO} (mils)	α=150 ΔE (keV)	α=150 ΔR_{EO} (mils)	α=138 ΔE (keV)	α=138 ΔR_{EO} (mils)	α=120 ΔE (keV)	α=120 ΔR_{EO} (mils)	α=90 ΔE (keV)	α=90 ΔR_{EO} (mils)
14	0.(V)	25.	43.	25.	45.	25.	45.	25.	44.	23.	40.
	180.(H)	26.	49.	26.	51.	26.	51.	25.	50.	24.	46.
	30.	28.	52.	27.	51.	27.	51.	27.	49.	27.	50.
	210.	29.	53.	28.	52.	28.	52.	28.	52.	27.	51.
	60.(H)	26.	51.	24.	49.	24.	49.	24.	49.	25.	50.
	240.(V)	26.	45.	25.	44.	25.	44.	25.	44.	26.	44.
	90.	23.	43.	23.	44.	23.	44.	23.	44.	22.	41.
	270.	24.	42.	24.	44.	24.	44.	24.	43.	22.	41.
21	0.(V)	28.	39.	29.	42.	29.	41.	28.	41.	26.	37.
	180.(H)	28.	44.	29.	47.	29.	47.	28.	46.	26.	43.
	30.	32.	49.	32.	48.	32.	48.	32.	49.	32.	48.
	210.	33.	49.	32.	49.	32.	49.	32.	50.	32.	48.
	60.(H)	29.	47.	28.	46.	28.	46.	28.	46.	29.	47.
	240.(V)	29.	41.	28.	40.	28.	40.	28.	41.	29.	41.
	90.	25.	38.	26.	40.	26.	40.	26.	40.	24.	38.
	270.	25.	37.	26.	39.	26.	39.	26.	39.	25.	37.

TABLE IV.--λ and λ_x at $\theta=\theta_{or}$ and $\theta=\theta_{or}+\pi$ for the same cases as shown in Table III.

		N=3 h=1 E_1=143 keV/turn $\Delta\phi=\pm2^o$									
		α=180		α=150		α=138		α=120		α=90	
τ	θ_{or}	λ (mils)	λ_x (mils)	λ (mils)	λ_x (mils)	λ (mils)	λ_x (mils)	λ (mils)	λ_x (mils)	λ (mils)	λ_x (mils)
14	0.	34.	-23.	36.	-26.	24.	-19.	7.	-6.	49.	14.
	180.	34.	29.	35.	30.	23.	20.	4.	3.	43.	-24.
	30.	25.	20.	33.	30.	31.	28.	29.	28.	20.	12.
	210.	35.	-23.	49.	-37.	47.	-36.	46.	-44.	34.	-22.
	60.	53.	46.	76.	68.	74.	67.	77.	70.	60.	56.
	240.	53.	-34.	75.	-53.	73.	-53.	76.	-56.	58.	-47.
	90.	16.	-12.	9.	-6.	4.	3.	29.	21.	81.	56.
	270.	11.	9.	5.	2.	6.	-6.	24.	-22.	61.	-52.
21.	0.	37.	-3.	38.	-7.	25.	-7.	10.	-10.	58.	-22.
	180.	26.	6.	25.	2.	17.	4.	10.	10.	49.	30.
	30.	28.	-5.	36.	0.	34.	-2.	34.	-6.	31.	-18.
	210.	24.	2.	37.	-7.	34.	-5.	31.	-2.	18.	11.
	60.	40.	1.	57.	11.	55.	12.	56.	14.	42.	18.
	240.	56.	0.	80.	-8.	77.	-9.	79.	-11.	57.	-16.
	90.	11.	-1.	4.	1.	8.	4.	30.	9.	73.	16.
	270.	12.	-3.	77.	-5.	7.	-5.	26.	-5.	70.	-2.

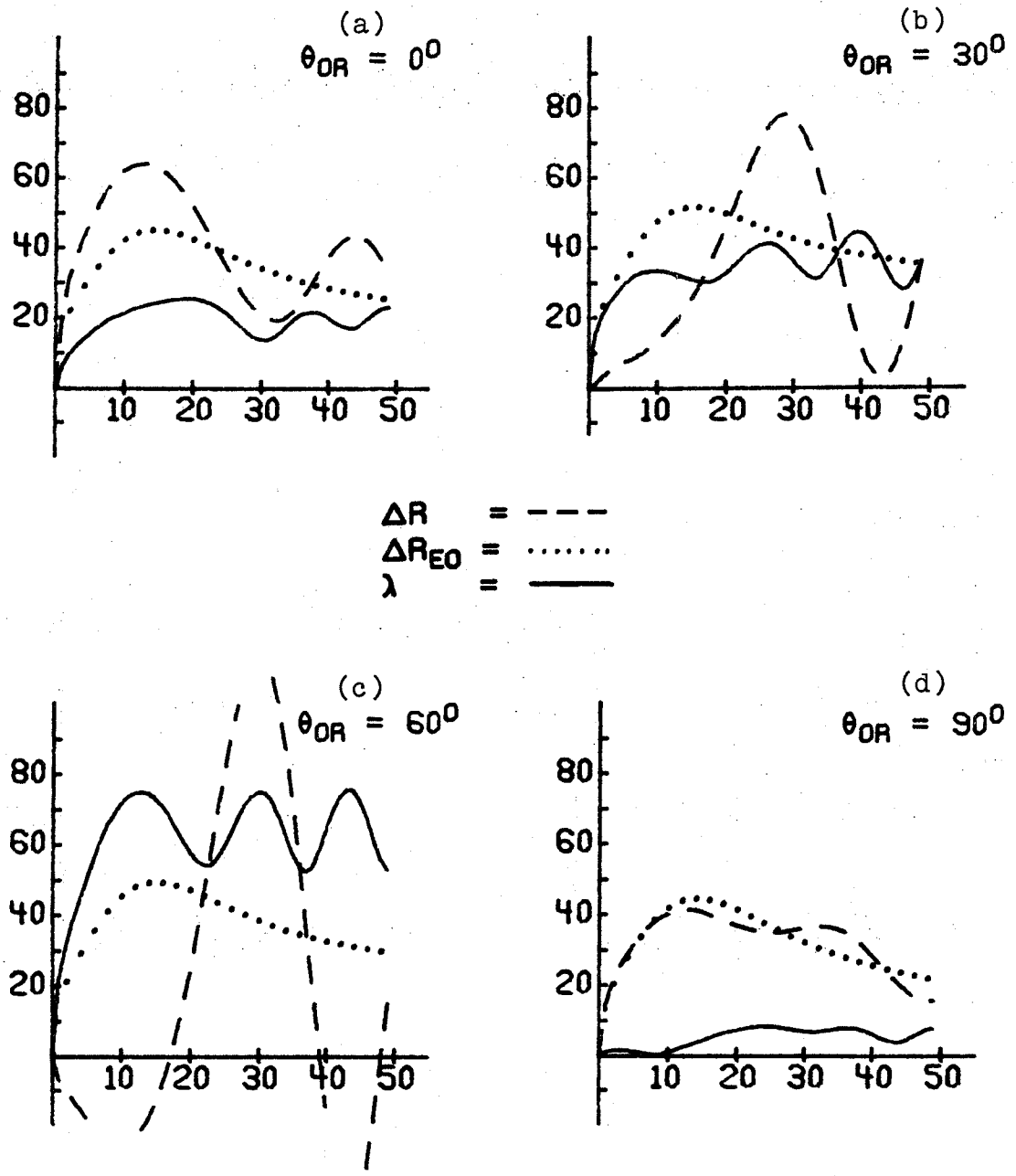

Figure 16. ΔR, ΔR_{EO} and λ vs. τ for N=3, E_f=30 MeV, τ_F=210, α=138° and h=1 plotted at $\theta=\theta_{or}$ for various θ_{or}'s. Ordinate values are in mils.

3.2 Fielder Phase Curves

In this section we shall investigate the effects of varying the magnetic field contour with a fixed dee geometry, our study here concerning the effects of the different $\phi_F(\tau)$ we may produce. We use the initial phase, $\phi_o \equiv \phi_F(\tau=0)$ and the turn number τ_o such that $\phi_F(\tau=\tau_o)=0$, to characterize these curves. In any real situation, one would locate the ion source so that the CR corresponds to the centroid of the maximum intensity ion group from the source. Thus a change in ϕ_o corresponds to a change in the source-puller location relative to θ_1. Changing τ_o at a fixed ϕ_o is a change in the magnetic field.

The five curves used here are presented in Fig. 17. The curve parameters (ϕ_o,τ_o) are: A=(10°,20), B=(20°,10), C=(20°,20), D=(20°,30), E=(30°,20). Curves going strongly negative on early turns are not considered because of the possible associated axial defocusing difficulties. An attempt was made in all cases to obtain the straightest possible line from ϕ_o to zero for $0 \leq \tau \leq \tau_o$ with Fielder. Behavior of $\phi_F(\tau)$ on the first few turns is dominated by the central cone which extends some three or four inches in radius and causes the initial rapid fall-off in phase observed for $\tau<3$. Control over all other sections of $\phi_F(\tau)$ is about as good as is possible since the average trim coil spacing at M.S.U. is nearly half the magnet gap (6.75 in.).

To obtain the data on ΔR_{EO} in Table V and on λ and λ_x in Table VI, we performed the procedure outlined in Sec. 2.2 for protons in three sector fields with E_f=30 MeV, α=138°, θ_{or}=0° and 60° and E_1=143 keV/turn. The columns labeled "Area" in Table V contain the results of using Eq. (8) and the different $\phi_F(\tau)$'s with trapezoidal rule integration. The values in parentheses in each column are "normalized" with the corresponding values for case E (note 1's in those columns). These normalized values of $\Delta R_{EO}(\theta_{or}=0^{\circ})$, $\Delta R_{EO}(\theta_{or}=60^{\circ})$ and "Area" should be the same for a given $\phi_F(\tau)$ if Eq. (8) is accurate. Agreement averages about 5% except for case A where 20% to 30% differences are average. Since all beams are similarly well centered, it should not be unexpected that the $\delta\phi_{CD}$'s are of similar magnitude in all cases. In case A, this means that on the very first turns ϕ_{CR} at θ_1 and θ_3 will be negative, decreasing ΔR_{EO} and accounting for the apparent discrepancies. Such evidence leads us to say that Eq. (8) is valid and useful.

The λ's of Table VI show that $\phi_F(\tau)$ for τ<10 or so is a most important characteristic and that the final λ is rather insensitive to the fine details of the $\phi_F(\tau)$ curves. Roughly one may group cases A with B, C and D, leaving E by itself, using the effect on λ as the distinguishing feature. From Fig. 17 it is seen that this grouping also is a rather natural one for the average of the $\phi_F(\tau)$'s,

TABLE VI.--λ and λ_x at $\theta=\theta_{or}=0^{o}$ and $\theta=\theta_{or}=60^{o}$ for the same cases as shown in Table V.

		N=3 h=1 $\alpha=138^{o}$ E_1=143 keV/turn $\Delta\phi=\pm2^{o}$									
		CASE A		CASE B		CASE C		CASE D		CASE E	
τ	θ_{or}	λ (mils)	λ_x (mils)	λ (mils)	λ_x (mils)	λ (mils)	λ_x (mils)	λ (mils)	λ_x (mils)	λ (mils)	λ_x (mils)
5	0.	10.	-10.	12.	-12.	14.	-14.	16.	-16.	24.	-24.
	60.	45.	44.	42.	40.	45.	43.	51.	50.	59.	58.
10	0.	16.	-15.	16.	-15.	21.	-21.	21.	-20.	34.	-32.
	60.	62.	60.	60.	60.	69.	68.	72.	70.	87.	85.
15	0.	18.	-14.	18.	-15.	24.	-18.	24.	-17.	38.	-29.
	60.	60.	51.	66.	61.	74.	63.	71.	60.	93.	83.
20	0.	19.	-8.	20.	-10.	26.	-10.	24.	-8.	41.	-16.
	60.	47.	12.	56.	31.	61.	24.	56.	19.	80.	45.

TABLE VII.--Comparison of ΔR_{EO} and λ for $\alpha=180^{\circ}$ and $\alpha=90^{\circ}$ at $\theta=\theta_{or}=0^{\circ}$ and $\theta=\theta_{or}=60^{\circ}$ to show a connection between α, θ_{or} and $\phi_F(\tau)$. See Fig. 17 for the corresponding $\phi_F(\tau)$ curves.

		N=3	h=1	E_1=143 keV/turn		$\Delta\phi=\pm2^{\circ}$	
			CASE A		CASE C		CASE E
α	θ_{or}	τ	ΔR_{EO} (mils)	λ (mils)	ΔR_{EO} (mils)	λ (mils)	ΔR_{EO} (mils)	λ (mils)
180.	0.	5	8.	19.	28.	16.	50.	16.
		10	14.	29.	40.	27.	66.	30.
		15	16.	37.	43.	34.	70.	38.
		20	15.	41.	41.	38.	66.	43.
	60.	5	12.	31.	34.	37.	60.	52.
		10	18.	46.	47.	53.	73.	80.
		15	20.	47.	51.	53.	78.	87.
		20	18.	37.	49.	43.	74.	73.
90.	0.	5	1.	25.	23.	21.	48.	16.
		10	7.	38.	36.	34.	67.	25.
		15	9.	54.	40.	49.	73.	40.
		20	9.	61.	39.	58.	70.	50.
	60.	5	3.	35.	25.	39.	49.	44.
		10	11.	49.	42.	57.	74.	67.
		15	15.	50.	50.	60.	83.	74.
		20	15.	38.	49.	48.	81.	64.

TABLE VIII.--Location and magnitude of the first maxima in ΔR_{EO} and λ at $\theta=\theta_{or}=0^{\circ}$ and $\theta=\theta_{or}=60^{\circ}$ for the $\phi_F(\tau)$ curves in Fig. 17.

N=3	h=1	$\alpha=138^{\circ}$	$E_1=143$ keV/turn		$\Delta\phi=\pm2^{\circ}$
CASE	θ_{or}	ΔR_{EO}		λ	
		Turn	Value (mils)	Turn	Value (mils)
A	0.	14	12.	19	19.
	60.	15	15.	13	63.
B	0.	9	26.	21	20.
	60.	10	29.	15	66.
C	0.	15	45.	19	26.
	60.	16	49.	13	75.
D	0.	19	57.	18	24.
	60.	19	62.	13	74.
E	0.	15	72.	20	41.
	60.	15	77.	14	93.

after it reaches its maximum, ΔR_{EO} should vary roughly as $(E_1)^{-\frac{1}{2}}$ at a fixed τ by Eqs. (7) and (8). Notice also that, while decreasing E_1 should decrease the resonant driving "force" acting to increase λ, it will also maintain ϕ_{CR} at a higher value over more turns, increasing the resonant drive. Therefore, Q is not a sensitive function of E_1 and increasing E_1 cannot be expected to improve Q greatly.

The second alternative is to maintain $\phi_F(\tau)$ as constant. Doing so introduces a rather subtle effect so we therefore present Table IX comparing data on $\phi_F(\tau)$, x, p_x (for the CR) ΔR_{EO} and λ for protons with E_f=30 MeV and E_1 values such that τ_F=120, 210, and 300. Since the $\phi_F(\tau)$ curves are the same (at least near the machine center), the integral in Eq. (8) is constant and ΔR_{EO} should vary as $(E_1)^{\frac{1}{2}}$, which can be verified as true from the table entries. Values of λ should likewise change by this factor since all resonance driving terms are combinations of terms similar to the left hand side of Eq. (7). However, ΔE depends on the $\delta\phi_{CD}$'s of Eq. (3). The x-p_x data included in Table IX shows that centering improves with increasing τ_F, as should seem intuitively correct, but more slowly than as $(E_1)^{\frac{1}{2}}$. Then $\delta\phi_{CD}$, at a given gap and τ, actually tends to decrease with decreasing τ_F since the denominator of Eq. (3) increases faster than the numerator. This decreases the rf asymmetry driving term, at a rate other than proportional to $(E_1)^{\frac{1}{2}}$. It is this difference in rates, between the

variations with E_1 in the l.h.s. of Eq. (7) at a constant $\phi_F(\tau)$ and in $\delta\phi_{CD}$ that gives rise to the larger λ values for τ_F=210 compared with either of the other cases.

Inspection of the data also shows that the 210 turn geometry is possibly close to producing the largest possible λ's under the condition of fixed $\phi_F(\tau)$. Since Q is insensitive to τ_F (the table shows only a 20% variation with a factor of 2.5 change in τ_F), no computer time was spent attempting to find this optimal τ_F. It is interesting to note, however, that in this case, as for constant $\phi_F(E)$, Q does not increase monotonically with E_1 as might be expected at first glance.

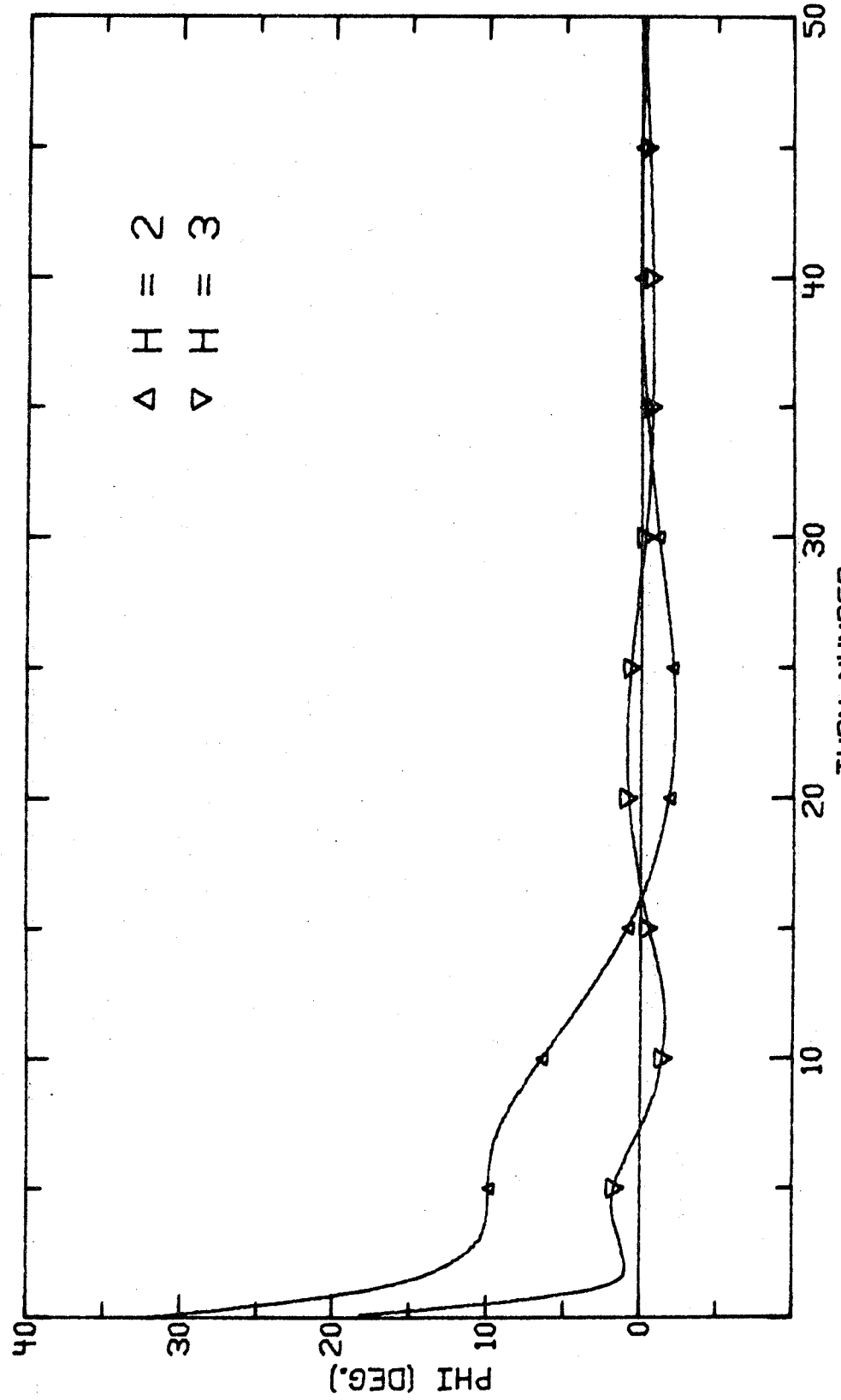

Figure 18. $\phi_F(\tau)$ for an M.S.U. deuteron field for h=2 and E_f=15 MeV and an M.S.U. C^{3+} field for h=3 and E_f=27 MeV.

The $\delta\lambda$'s at opposing gaps are almost equal, differing mainly only by the energy denominator of Eq. (7), and, therefore, nearly cancel. As a measure of the orbit symmetry involved, Fig. 19 gives p_x asymmetry values for AEO's with $\alpha=138^o$ vs. percentage of E_f on h=1, 2 and 3. By Sec. 2.3 we expect values for $\alpha=90^o$ to be lower than the h=2 curve actually plotted, which is already lower than the h=1 case presented for comparison.

Of greater interest is a comparison of ΔR_{EO} and λ data for 138^o dees and h=2 in Table X and previously given data for h=1 (Tables III, V and VI). The h=2 ΔR_{EO} data shows larger variations (approximately twice as large) with θ_{or} as follows from the more important form factor phase shifts. As to the data on λ, note first that h=2 does not demonstrate variations with θ_{or} as large as does h=1, nor does it have the very strong preference (in terms of larger Q_x) for $\theta_{or}=60^o$ and the poor showing at $\theta_{or}=90^o$ discussed before for h=1. In fact, $\theta_{or}=90^o$ gives the best Q_x on h=2.

To understand these results one must realize that the zero phase gap crossings occur as in Fig. 20. (Cf. Fig. 9.) Large phases now tend to produce small $\delta\lambda$'s at θ_1 and large $\delta\lambda$'s at θ_2, in direct contrast to the h=1 situation. Small phases are now to be preferred at θ_1 for larger resonant increase in λ. The better Q_x for $\theta_{or}=90^o$ may now be seen to be connected with the very low phase occurring at gap 1 and the very large phase at gap 3. The reversal in relationship between θ_{or} and λ is the reversal in the sign of

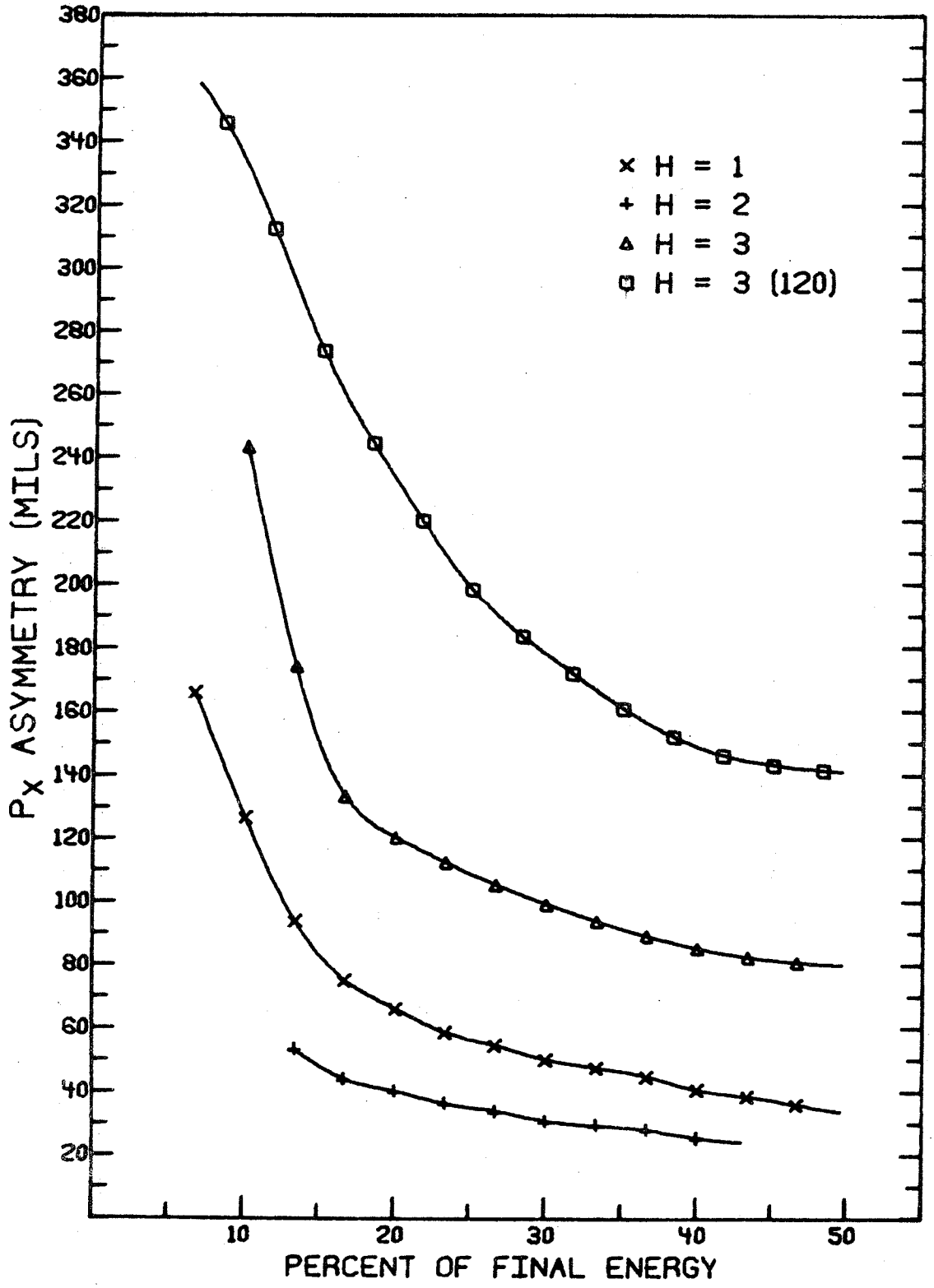
380
360
340
320
300
280
260
240
220
200
180
160
140
120
100
80
60
40
20
P_X ASYMMETRY (MILS)
× H = 1
+ H = 2
△ H = 3
□ H = 3 (120)
10
20
30
40
50
PERCENT OF FINAL ENERGY

Figure 19.

dV_{rf}/dt at each gap when comparing h=1 and h=2.

Again referring to Fig. 19, we see that AEO asymmetry greatly increases with third harmonic operation. This, along with the fact that $\delta\phi_{CD}$ now includes a factor of three, makes acceleration very difficult in some cases and impossible in others: one finds that one cannot decelerate particles backward past 1 or 2 MeV to find source positions using $\alpha=138^{o}$ and $\tau_F=210$. As demonstrated by Learn, et al.,[15] we may expect 90^{o} dees to perform adequately if we switch to a 120 turn geometry although 138^{o} dee performance is still unsatisfactory as supported by the large asymmetries in Fig. 19. (We should mention that our difficulties on h=3 stem from our centering requirement for the CR.) We shall, therefore, consider only $\alpha=180^{o}$ and 90^{o} for h=3 and will, for convenience, use the same field as Learn. For further details on this problem and the performance of 60^{o} dees, we refer the reader to Learn, et al.

The relevant data is contained in Table XI for 27 MeV C^{+3} ions. Again we see the dependence of ΔR_{EO} on θ_{or} becoming stronger from the form factor effect for both $\alpha=180^{o}$ and 90^{o}. The extremely large λ values observed (as much as an order of magnitude greater than most of our previous cases) are due partially to the increased sensitivity to the gap-crossing resonance shown in Fig. 19 and partially to values of $\delta\phi_{CD}$ of 20^{o} to 30^{o} between gaps on early turns. This is also, of course, the reason for the order of magnitude change in λ between $\theta_{or}=30^{o}$ and 90^{o}.

In summary we can say that Q is highly dependent on h because of the different gap crossing times involved at fixed α. A phase selection system which works well on one harmonic should not be expected to perform satisfactorily on other harmonics. For example, with 90^{o} dees, citing the best values at any turn in each case one finds $Q(h=1)/Q(h=2) \simeq 4$ at $\theta_{or}=0^{o}$.

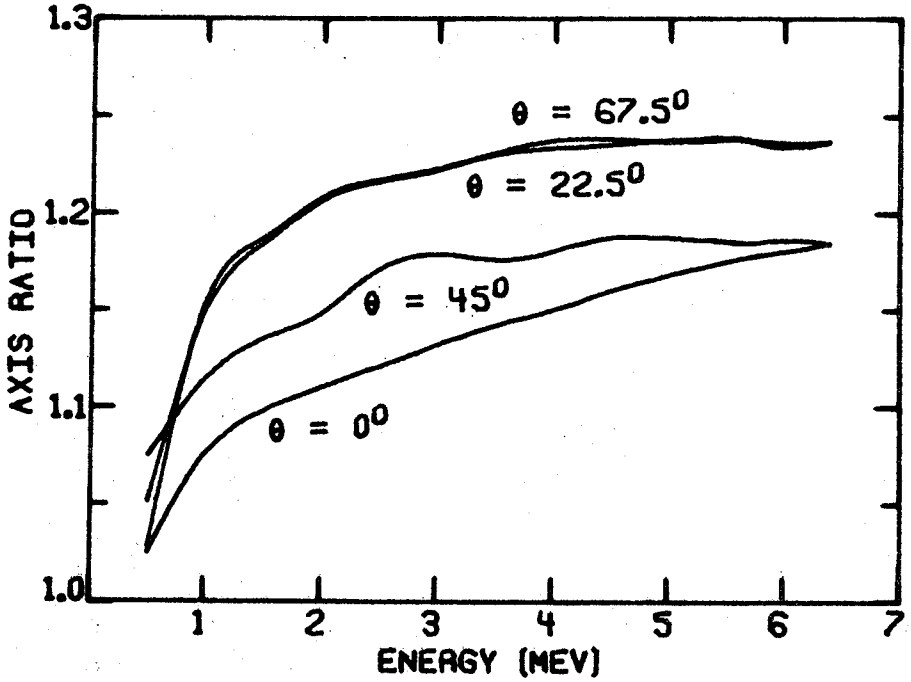

Figure 22. Eigen-ellipse axis length ratios vs. energy for a proton field with N=4, E_f=30 MeV. Note change of ordinate scales from Fig. 14.

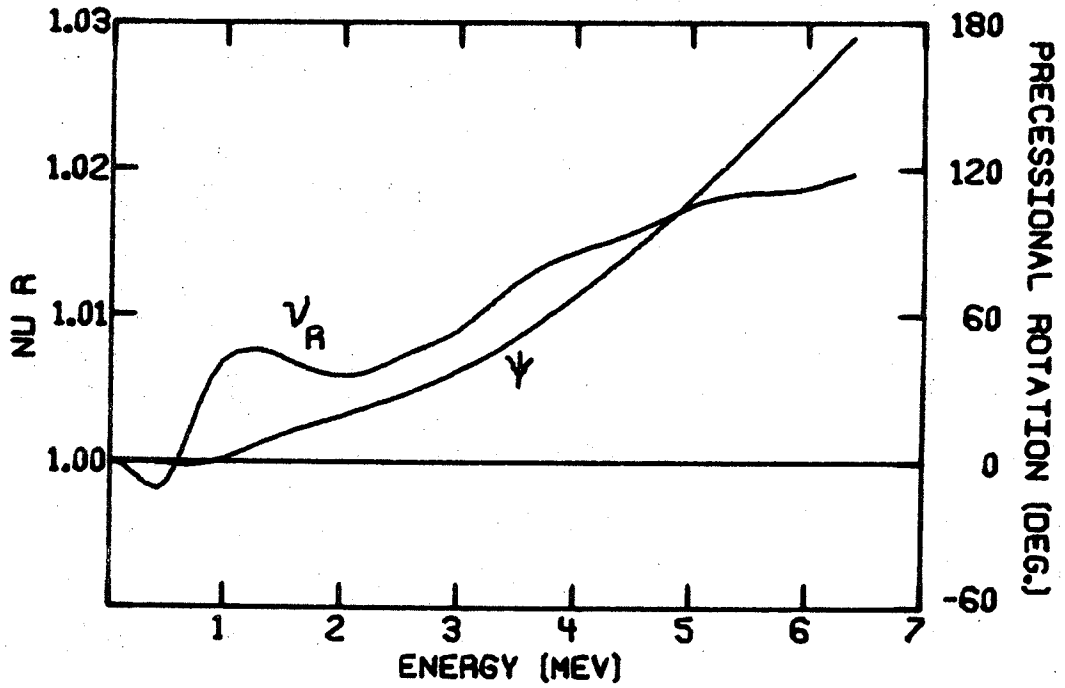

Figure 23. ν_r and ψ(see Eq. 11) vs. energy in the field used for Fig. 22. Note change of ordinate scales from Fig. 15.

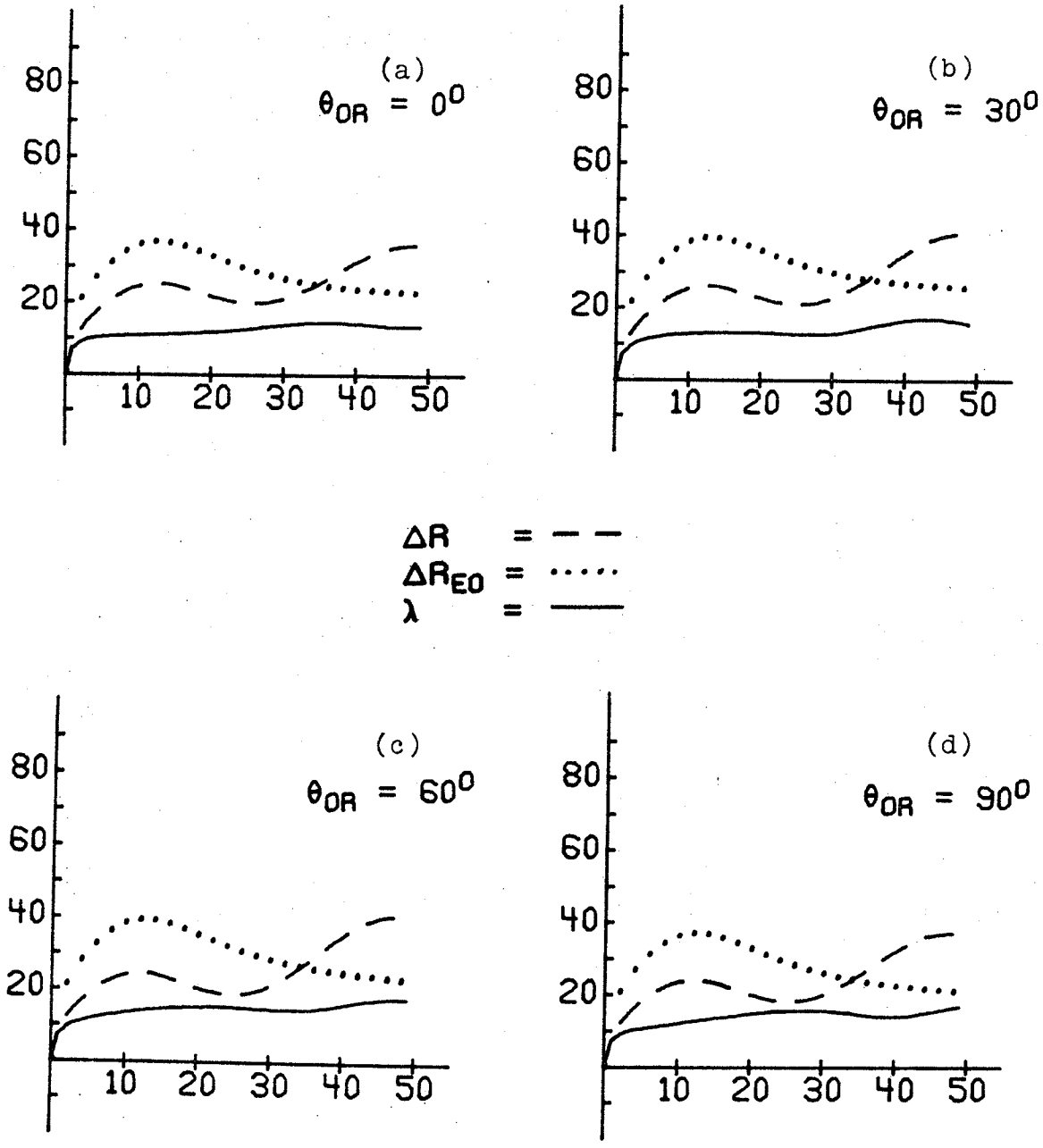

Figure 24. ΔR_{EO}, λ and ΔR vs. τ plotted at $\theta=\theta_{or}$ for various θ_{or}'s for N=4, E_f=30 MeV, $\alpha=138^{\circ}$, τ_F=210 and h=1. Ordinate values are in mils.

optimizing Q. Only for 90^{o} dees is there a strong dependence of ΔR on anything other than energy difference and this is independent of θ_{or}. Even after correcting for the difference in $\phi_F(\tau)$ curves, the best possible Q for N=4 will be seen to be worse than the best for N=3.

These same general statements should also apply to higher harmonic operation. One further effect we would find is lessening of the variations in ΔR_{EO} with θ_{or} because the form factor $F(\theta)$ varies as N^{-2}.

$$Q_{EO} = \Delta R_{EO}/\Delta\phi = -(R_o/2)\langle\phi_F\rangle_\tau(1 + F(\theta)) \qquad (12)$$

an expression which the data in Sec. 3.2 showed to be fairly accurate. To apply Eq. (12) to all azimuths, one must require that δR_{EO} from Eq. (7) at any gap is much less than ΔR_{EO} used above. We shall assume that τ is large enough for such to be the case so that Q_{EO} is independent of θ in all our discussion in this section.

In the other cases, e.g., $\alpha=90^o$, $\theta_{or}=90^o$, N=3, h=1 or $\alpha=90^o$, $\theta_{or}=30^o$, N=3, h=3, where λ and ΔR_{EO} are of comparable magnitude, they must be added, with due consideration given to the orientation of Λ, to determine the optimal slit location. In the examples previously given in Figs. 16 and 24, we have included the end results of these considerations: ΔR vs. τ. Tabulated results in the form of Q values fill Tables XIII, XIV and XV. Maxima in these curves obviously are optimal slit locations, but the curves are accurate only near the azimuths at which they are drawn. Since we are formally presenting data only at $\theta=\theta_{or}$ (Sec. 5.3 contains data at other angles), we must discuss the principles governing these curves so we may have a basis for deciding what ΔR will be at arbitrary angles.

At this point we return to the data on λ_x which has been supplied in most of the tables of Chapter 3 but has not been formally discussed. These λ_x depend not only on λ, which we have talked about at length, but also on the orientation of Λ in x-p_x space. For $\alpha=180^o$, before the

TABLE XIV.--Turn number and value of the best Q at $\theta=\theta_{or}$ and $\theta=\theta_{or}+\pi$ for various dee angles on h=2 and h=3. This table complements Tables X and XI.

θ_{or}	N=3 h=2 E_1=68 keV/turn $\alpha=138^\circ$		$\alpha=90^\circ$		N=3 h=3 E_1=227 keV/turn $\alpha=180^\circ$		$\alpha=90^\circ$	
	τ	Q (mils/deg)	τ	Q (mils/deg)	τ	Q (mils/deg)	τ	Q (mils/deg)
0.	9	9.1	10	7.9	9	28.0	18	18.6
180.	25	17.1	12	7.9	9	-32.0	17	-38.4
30.	8	3.6	10	10.4	8	-14.0	18	110.6
210.	18	18.6	15	12.5	8	27.0	19	-89.8
60.	10	15.6	22	10.1	9	-31.5	18	-33.7
240.	10	6.5	13	9.6	8	28.6	18	-33.7
90.	15	17.1	9	7.7	7	16.0	26	-13.0
270.	34	12.8	11	7.4	8	-19.5	9	-10.0

precession angle ψ becomes large, Λ parallels the x axis. However, for any other α, the interactions represented by the vectors K_1 and K_2 in Eq. (9) cause Λ to take on some other orientation. The sign of λ_x results from the dependence of ϕ_{CR} on gap number. For example, in Fig. 16 ΔR may be seen to start as the sum of the other two curves for $\theta=0^o$ and 90^o ($\lambda_x \leq 0$) and their difference for $\theta_{or}=30^o$ and 60^o ($\lambda_x \geq 0$).

If we define μ as the angle between Λ and the x axis so that we could calculate it as $\mu=\text{Tan}^{-1}(\lambda_p/\lambda_x)$, we find that $\mu \simeq \mu_o$, a constant, over the early turns until precession takes over. Given such a μ_o at $\theta=0$, for instance, on a turn where ψ is small, one may rewrite Eq. (4) as

$$\Delta R(\theta,\tau) = \Delta R_{EO}(\tau) + \lambda(\tau)\ \cos(\nu_r\theta-\mu_o+\psi(\tau)). \qquad (13)$$

This equation is particularly useful for τ large enough (usually $\tau>10$) that ΔR_{EO} is independent of θ and λ varies only according to eigen-ellipse effects. With Eq. (13) and the data in Chapter 3, one can now determine ΔR at any location in his machine. (Strictly speaking, given only the data in Chapter 3, one must resolve the sign ambiguity involved with $\mu_o=\text{Cos}^{-1}(\lambda_x/\lambda)$ by obtaining the difference between μ_o and μ on some later turn and comparing that difference to the $\Delta\psi$ expected for the corresponding $\Delta\tau$.)

One assumption implicit in the discussion of this section is that we are dealing with separated turns. In fact, such would not be the case for τ=20-30, where we would place our slits, because of the large beam phase width to that point. To cure this problem, the M.S.U. cyclotron contains a slit (10 mils wide for h=1 proton operation) about 180° away from the source-puller. This "half turn" slit performs a rough phase selection, passing at most two particle groups at different centroid phases, each with a relatively narrow phase width. One group is the maximum intensity group, the centroid of which corresponds to our CR. It is this group which the cyclotron is tuned to accelerate and on which our slits perform the final phase selection. The other group is lost on the jaws of the first slit, the difference in centroid phases not being enough to cause overlapping of turns.

One final comment to be made concerns the minimum practical slit width which should be used in any system. Certainly, one can obtain arbitrarily good phase resolution in one's beam by decreasing his slit width, but at the cost of decreased beam current. In fact, if one assumes that ΔR varies linearly with $\Delta\phi$, it is easy to show that the beam phase width decreases (improves) at nearly the rate at which beam current decreases as slit width is decreased, until the slit width is about the same as the zero-energy-spread beam width. This latter is just the x width of the

4.2 Comparison with "Cyclone"

As mentioned in Sec. 2.2, Devil suffers from one major simplification: the neglect of the exact electric fields on the first few turns. The justification for this neglect is that such fields are different for each central region design, even for equal dee angles. It is also, of course, important to separate other influences on Q from the effects of these electric fields. However, this study could in no way be called complete without some comparison, albeit brief, of results from Devil with those from "Cyclone,"[16] an orbit code utilizing measured electric potential data for the source-puller and early turn regions.

Figure 25a gives Cyclone results for ΔR_{EO}, λ and ΔR vs. τ at $\theta=0^{o}$ for a value of $\omega_{RF}t_{o}=-22^{o}$ for the CR at the source. The E_f of 42 MeV and the central region geometry were chosen to correspond to data previously published by Blosser.[5] Devil results for this case are in Fig. 25b. ΔR_{EO} may be seen to be the same in both cases as expected since ϕ_{CR} from Cyclone agrees with ϕ_{CR} from Devil at $\theta=0^{o}$ and 180^{o} to within about 1^{o}. The Cyclone λ is smaller than its Devil counterpart by a factor of about 0.5. Note, however, that the extrema in the ΔR curves occur at similar τ values in both cases, the Cyclone values peaking near $\tau=18$ and Devil values near $\tau=14$.

The differences in λ may be traced to the more gradual nature of the energy gain on early turns in Cyclone. Our

picture of discrete $\delta\lambda$'s is no longer valid and must be replaced by one in which the change in λ is spread over some rotation angle at each gap crossing. But since disjunction acts only parallel to the x axis, it should be expected that the net effective $\delta\lambda$ will be less than the discrete $\delta\lambda$ we have discussed before. The discrepancy in extrema locations is also a function of the details of the electric fields. The μ_o from Cyclone has Λ about midway between the axes ($\mu_o \simeq -45^o$) while that from Devil has Λ closer to the positive x axis ($\mu_o \simeq 0^o$). This orientation difference must be made up by precession, hence the extra turns required to bring Λ parallel to the x axis, the extremal condition.

Figure 25c shows the Devil results for ΔR and its components in this 42 MeV case at $\theta=180^o$. Comparison with Fig. 3 in the work of Blosser cited above shows the same agreement as between Figs. 25a and b. Note also the exchange of node and antinode locations in ΔR between Figs. 25b and c and between Fig. 25a and Blosser's Fig. 3. This follows directly from Eq. (12) with a change in θ of 180^o. We also show Fig. 25d with ΔR and its components for a ray displaced by δp_x from the CR. This should be compared with Blosser's Fig. 5 to show that Devil and Cyclone agree on the location for a slit to eliminate spatially displaced particles.

Q larger. This also means that three sector cyclotron have a definite advantage over their four sector counterparts when it comes to performing phase selection. (See Sec. 3.5.)

In particular, N=3 cases are sensitive to θ_{or}. As the dees are rotated with respect to the magnetic field, CR centering is modified, altering ϕ_{CR} and, ultimately, λ. Thus we observe as much as an order of magnitude change in λ ($\alpha=138^{o}$, h=1 and $\alpha=90^{o}$, h=3) as θ_{or} changes to sweep the dee symmetry line through one sector. $\theta_{or}=60^{o}$ tends to give the best h=1 results for most dee angles ($\theta_{or}=90^{o}$ is best for $\alpha=90^{o}$), while results on other harmonics are mixed, being highly α dependent. (See Sec. 3.1.)

Improvement in Q may be brought about in most cases by having $\phi_{F}(\tau)$ stay as large positive as possible throughout the region herein ν_{r} is close to one. This increases ΔR_{EO} and usually also λ, but exceptions there do arise ($\alpha=90^{o}$, $\theta_{or}=0^{o}$, h=1) because disjunction is not linear with ϕ_{CR}. Thus, a central field cone may be seen to be beneficial for phase selection. It should be borne in mind that having $\phi_{CR}(\tau)=0$ for all τ is not really the necessary condition for obtaining minimum final energy spread, although it is sufficient. The necessary condition is that the integral,[1]

$$\int_{0}^{E_f} (\sin\phi/\cos^{3}\phi)\,dE = 0.$$

Thus, large regions of large positive phase are not detrimental to final energy spread if eventually balanced by regions of negative phase. This condition is always

APPENDICES

5.1 Formula Derivations

5.1.1 Calculation of the Starting Condition for an Accelerated Equilibrium Orbit

In x-p_x phase space, the point representing a freely coasting particle rotates about the origin. At an accelerating gap the point jumps in the negative x direction a distance equal to the EO radial shift corresponding to the energy gain ΔE. This shift, ΔR_{EO}, is given in Sec. 2.4. Let us neglect $F(\theta)$ and assume that $(E)^{-\frac{1}{2}}$ varies negligibly over any one turn so that ΔR_{EO} depends only on ΔE. Further assuming a two dee system with dee angle α less than 180^o (one or two dees of 180^o is just a simplification of the argument below), a constant phase ϕ within a turn, harmonic h=1 and setting $E_g = qV_d$ we may write the energy gains at the gaps as

$$\Delta E_1 = \Delta E_3 = E_g \cos(\pi/2-\alpha/2+\phi) = E_g \sin(\alpha/2-\phi)$$

$$= E_g (\sin(\alpha/2)\cos\phi - \cos(\alpha/2)\sin\phi)$$

$$\Delta E_2 = \Delta E_4 = -E_g \cos(\pi/2+\alpha/2+\phi) = E_g \sin(\alpha/2+\phi)$$

$$= E_g (\sin(\alpha/2)\cos\phi + \cos(\alpha/2)\sin\phi).$$

If we define

$$\delta = A(2E_oE)^{-\frac{1}{2}} E_g \sin(\alpha/2)\cos\phi$$

$$\varepsilon = A(2E_oE)^{-\frac{1}{2}} E_g \cos(\alpha/2)\sin\phi \ ,$$

One should observe that, under our assumptions, the geometry repeats after ½ turn so $X(\pi) = X(0)$ by symmetry. This condition also yields the same $X(0)$ as above.

$$\Delta E = -(\Delta\phi)\ E_g \sin(\alpha/2) \sum_{\tau} \sum_{i} \phi_i(\tau). \qquad (14)$$

If we replace $E_g \sin(\alpha/2)$ by $E_1/4$, then this result holds for any h.

We may use the Euler-Maclaurin formula to replace the sum over τ by an integral as follows:[17]

$$\sum_{\tau=\tau_j}^{\tau_f} \phi_i(\tau) \simeq \int_{\tau_j}^{\tau_f} \phi_i(\tau)\, d\tau + \tfrac{1}{2}(\phi_i(\tau_j)+\phi_i(\tau_f)).$$

In the cases we are interested in, $\tau_j=0$ and τ_f is usually greater than 15 so that $\int \phi_i(\tau)\, d\tau >> \phi_i(\tau_j)$ and $\phi_i(\tau_f)\simeq 0$.

If we recognize that $\phi_F(\tau)$ is nearly the average value of the $\phi_i(\tau)$ over one turn and replace $E_g \sin(\alpha/2)$ by $E_1/4$, Eq. (7) in Sec. 2.5 follows immediately from Eq. (14).

Cyclotron Lab's XEROX SIGMA-7 computer, which has 64K words of real core. Average running time accelerating five rays for 50 turns with six output azimuths and creating three plots is about 7.5 minutes.

F. (2I2, F12.5)

0 1 Frequency scale factor, default=1

0 2 ε_{rf}

0 3 Acceleration harmonic

0 4 Dee-To-Ground Voltage (kV)

0 5 θ_{or}

0 6 α_1

0 7 α_2

0 8 Phase constant for h≠1, default=90^{o}(h=2), -180^{o}(h=3)

0 9

010 Ray ID (see below) at Λ vector origin

011 Ray at Λ vector head

012 Number (maximum=6) of plotting angles to follow
-0, no plotting done, skip to next input
a.) (4A4) Plot Title
b.) (7F11.5) Plotting angles (degrees)

013 Number (maximum=105) of values in following EO table
=0, no table follows, skip to next input
a.) (F11.5) Angle for which EO data is presented
b.) (3F12.5) EO table (E, R_{EO}, P_{REO})

014 Number (maximum=16) of extra printing angles to follow.
Dee gaps are automatically included.
a.) (7F11.5) Output angles

Initial (source) conditions

G. (2I2, F12.5)

ID, IN, Z
where
ID = Ray identification number
= 1 implies CR (value of Z copied into variable IN for all other rays when this ID occurs)
IN = Variable index

LIST OF REFERENCES

REFERENCES

1. M. M. Gordon, "Single Turn Extraction," IEEE Trans. Nucl. Sci. NS-13 (4), 52(1966).

2. H. G. Blosser, M. M. Gordon and T. I. Arnette, "Resonant Extraction from Three-Sector Low-Spiral Cyclotrons," Nucl. Instr. and Meth. 18-19, 488(1962).

3. H. G. Blosser, "Problems and Performance in the Cyclotron Central Region," IEEE Trans. Nucl. Sci. NS-13 (4),1(1966)

4. H. G. Blosser, "Performance of a Modern Medium Energy Cyclotron," Bull. Am. Phys. Soc., (Nov. 1967).

5. H. G. Blosser, "Optimization of the Cyclotron Central Region for the Nuclear Physics User," Fifth International Cyclotron Conference (Butterworths, London, 1971), 257.

6. D. W. Kerst and R. Serber, "Electronic Orbits in the Induction Accelerator," Phys. Rev. 60, 53(1941).

7. E. D. Courant and H. S. Snyder, "Theory of the Alternating-Gradient Synchrotron," Ann. Phys. (N.Y.) 3, 1(1958).

8. M. M. Gordon, "Orbit Properties of the Isochronous Cyclotron Ring with Radial Sectors," Ann. Phys. (N.Y.), 50, 571(1968).

9. A. J. Lichtenberg, Phase Space Dynamics of Particles. (John Wiley & Sons, Inc., New York, 1969), p. 119.